Revista Brasileira de Ciência do Solo

Division - Soil in Space and Time | Commission - Soil Genesis and Morphology

Genesis of Soils from Bauxite in Southeastern Brazil: Resilication as a Soil-Forming Process

Ana Carolina Campos Mateus[(1)], Fábio Soares de Oliveira[(2)*], Angélica Fortes Drummond Chicarino Varajão[(1)], and Caroline Cibele Vieira Soares[(3)]

[(1)] Universidade Federal de Ouro Preto, Departamento de Geologia, Programa de Pós-graduação em Evolução Crustal e Recursos Naturais, *Campus* Morro do Cruzeiro, Ouro Preto, Minas Gerais, Brasil.
[(2)] Universidade Federal de Minas Gerais, Instituto de Geociências, Departamento de Geografia, Belo Horizonte, Minas Gerais, Brasil.
[(3)] Universidade Federal do Espírito Santo, Departamento de Geologia, Alegre, Espírito Santo, Brasil.

ABSTRACT: Pedological studies using X-ray diffraction (XRD), X-ray fluorescence (XRF), optical microscopy, and scanning electron microscopy (SEM-EDS) showed a Xanthic Ferralsol formed from the degradation of bauxite on a slope in the Caparaó region, in southeastern Brazil. We found a decrease in the number and size of bauxite fragments toward the top of the profiles, bauxite fragments that were more degraded at the top of the profiles, transformation of gibbsite into kaolinite, and absolute enrichment in silicon in the mass balance. These indicators suggest that resilication could be the major process responsible for formation of the soil; detailed studies are needed to verify the origin of the silica. The reintroduction of silica into the system occurs by the biogeochemical cycling of vegetation and, in some cases, water table fluctuations, highlighting the role of resilication as a soil-forming process in bauxite-derived soils.

Keywords: pedogenesis, Ferralsol, kaolinite, micromorphology.

***Corresponding author**
E-mail: fabiosolos@gmail.com

Received: November 15, 2016
Approved: May 12, 2017

How to cite: Mateus ACC, Oliveira FS, Varajão AFDC, Soares CCV. Genesis of soils from bauxite in southeastern Brazil: resilication as a soil-forming process. Rev Bras Cienc Solo. 2017;41:e0160507.
https://doi.org/10.1590/18069657rbcs20160507

INTRODUCTION

Most of the lateritic cover in the southeastern region of Brazil occurs in a large NNE-trending zone that comprises the Mantiqueira and Caparaó Ranges, which are associated with gneisses (Valeton and Melfi, 1988; Lopes and Carvalho, 1990; Valeton et al., 1991; Beissner et al., 1997) and granulitic rocks (Soares, 2013; Soares et al., 2014), respectively.

Studies conducted by the latter group of authors showed that the genesis of bauxite from charnockites occurred in different stages in accordance with the order of stability of the minerals, which characterizes the formation of an isalteritic horizon along the slope and explains the bauxitization process in the Caparaó Range, SE Brazil. The bauxites are located on steep slopes at elevations between 700 and 900 m and are always overlaid by Ferralsols. Although the studies of Soares (2013) and Soares et al. (2014) have shown important morphological features of the pedologic cover, the process responsible for its genetic affiliation has not been clearly defined.

Various models of aluminous duricrust profiles postulate that hard, fragmented, or massive bauxite facies are situated under pedologically friable soil horizons (Groke et al., 1980). Although some authors interpret the origin of these soil horizons as simultaneous to the formation of the bauxite, most understand that these horizons are the result of the geochemical degradation of bauxite from the growth of dense vegetation cover (Lucas et al., 1993). In this perspective, pedogenesis occurred on material that was already quite weathered, and not directly on fresh rock.

Resilication is one of the main processes that are associated with the degradation of bauxite (Lacroix, 1913; Harrison, 1934; Lacroix, 1934; Van der Marel, 1960; Keller and Clarke, 1984). The reincorporation of silica in a pedological system destabilizes some existing minerals, such as gibbsite, and neoforms others, such as kaolinite (Van der Marel, 1960; Tewari, 1963; Aleva, 1965; Valenton, 1974; Bocquier et al., 1982; Boulangé and Bocquier, 1983; Boulangé, 1984; Sigolo and Boulangé, 1987; Sigolo and Boulangé, 1989; Boulangé and Carvalho, 1989; Varajão et al., 1989, 1990; Lucas, 1997; Horbe and Costa, 1999; Oliveira et al., 2013a). Although resilication has been reported as a common process in the evolution of many bauxitic deposits, it has rarely been addressed as a soil-forming process. We highlight here the studies of Horbe and Costa (1999) that showed the genetic relation between Latosols and the lateritic crusts in the north of Brazil.

Resilication is the main process involved in the transformation of bauxite into soil and, therefore, can be approached as a pedogenetic process. However, considering the expressive distribution of soils on bauxite deposits of southeastern Brazil and aiming to contribute to the understanding of the genetic interrelationship between them, the present study emphasizes the morphological, mineralogical, and geochemical transformations that were involved in soil formation. To better develop the studies of geological mapping, geochemical prospecting, and land use in the southeast region of Brazil is of fundamental importance to define if the soils are autochthonous or allochthonous in relation to the bauxite.

MATERIALS AND METHODS

Study area

This study examines a slope that is located between the states of Minas Gerais and Espírito Santo, specifically, between the towns of Espera Feliz and Dores do Rio Preto (Figure 1a). Approximately 30 km north is the Caparaó National Park that contains the Pico da Bandeira, the third highest peak in Brazil, at 2891.98 m height (Figure 1b). Geologically, the area has granulitic rocks with mafic enclaves of the Juíz de Fora complex/Caparaó suite (Horn et al., 2007; Soares, 2013).

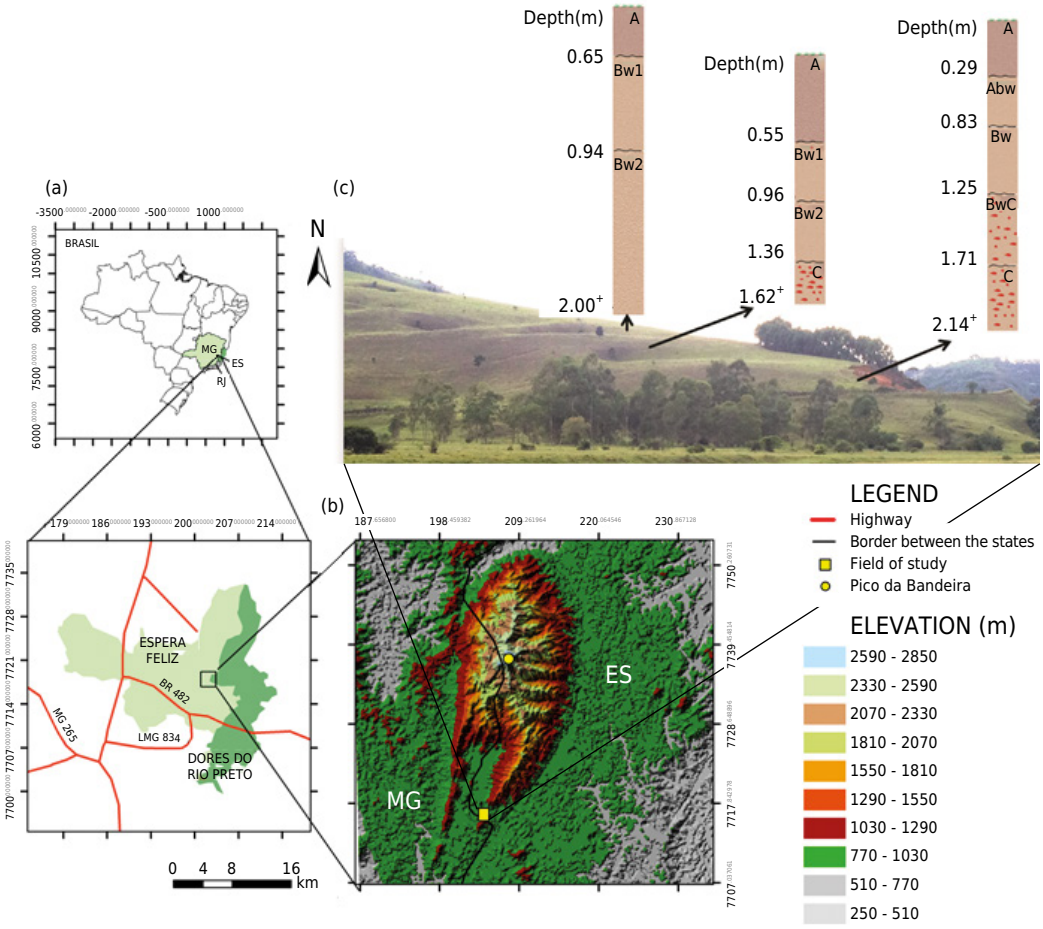

Figure 1. Location and access maps of the study area. (a) Main access routes to the towns of Espera Feliz, MG and Dores do Rio Preto, ES. (b) Location of the slope to the south of the Pico da Bandeira on an Aster image. (c) Slope image that shows the regions where the soil sampling pits were dug and describes the horizons and depths of profiles L1, L2, and L3.

Soil sampling

We studied three soil profiles along high (Ferralsol 1), intermediate (Ferralsol 2), and low (Ferralsol 3) slopes with depths of 2.00, 1.62, and 2.14 m, respectively (Figure 1c). Macromorphological descriptions of each profile were made according to Santos et al. (2013b). Soil colors were obtained by Munsell color charts (Munsell, 1975), and the profiles were classified according to the FAO System (Soil Survey Staff, 2014). A total of 11 disturbed samples and 7 undisturbed samples were collected for physical, chemical, mineralogical, and micromorphological analyses.

Physical, chemical, and mineralogical analyses

The physical, chemical, and mineralogical properties of the soil samples were analyzed. Particle size was determined by the total dispersion method according to Donagema et al. (2011). After vertical shaking for 16 h with sodium hexametaphosphate solution as a dispersant, the clay content was determined by the pipette method, the gravel and coarse and fine sand were separated by sieving, and silt content was obtained by the difference of the sum of the other fractions in relation to the original sample.

The pH was determined in water and in 1 mol L^{-1} KCl, which was measured potentiometrically at a soil:solution ratio of 1:2.5. Exchangeable bases (Ca^{2+} and Mg^{2+}) were extracted with 1 mol L^{-1} KCl at a soil:solution ratio of 1:10 and were quantified by atomic absorption spectrometry. Sodium and K were quantified by Mehlich-1 (0.05 mol L^{-1} HCl + 0.025 mol L^{-1} H_2SO_4) at a soil:solution ratio of 1:10 and determined by

flame photometry. Acidity was extracted with 1 mol L^{-1} KCl at a soil:solution ratio of 1:10 and titrated with 0.025 mol L^{-1} NaOH in the presence of a bromothymol blue indicator, which is expressed in exchangeable Al^{3+}. The H^{+} and Al^{3+} were extracted with 0.5 mol L^{-1} calcium acetate at pH 7.0 and titrated with 0.0606 mol L^{-1} NaOH with a phenolphthalein indicator. Total organic C (TOC) was determined according Yeomans and Bremner (1988).

Total chemical composition was determined by X-ray fluorescence (XRF - PAnalytical Philips Magix spectrometer with a PW2540 autosampler). Sodium, K, Mn, Mg, Ca, Fe, Al, Ti, P, and Si were analyzed, and their oxide contents were reported in wt %. An isoelement titanium (iso-Ti) estimate was made because titanium is considered one of the least mobile elements in alteration systems and, thus, better able to predict the relationship between geochemical loss and gain in the evolution of pedological cover. These values were used in the mass balance calculation according to Millot and Bonifas (1955).

The mineralogical compositions of total samples (sand, silt, and clay fractions), previously screened in the 2 mm mesh sieve and dried at 40 °C, were obtained by X-ray diffraction (XRD) with an Empyrean PAnalytical diffractometer with CuKα radiation in the range from 2° to 70° 2θ, with a step size of 0.02° 2θ and count of 10" per step. The XRD patterns were interpreted through use of HighScore X'Pert Plus software and patterns known from the literature (Brindley and Brown, 1980).

Micromorphological description

Thin sections of 11 soil samples, consisting of three bauxite fragments and eight from the pedological horizons, were used for the micromorphological descriptions. The friable samples were impregnated with Polilyte (Reforplás T208) polyester resin (Filizola and Gomes, 2004). Micromorphological studies were conducted under a Zeiss microscope together with a photographic camera, using terminology from Stoops (2003).

The morphological and chemical analyses of the samples were performed under a Scanning Electron Microscope (SEM-JEOL-JSM-5510) that was equipped with an energy dispersive X-ray spectrometer (Thermo Electron). The samples were coated with a thin layer of C and analyzed under an accelerated voltage of 20 kV and load current of 85 µA. A work distance of 20 mm was applied. The Si, Al, Fe, and Ti were analyzed and reported in oxides (% in weight).

Bulk density and geochemical loss and gain calculations

Apparent density was calculated on cubes with side dimensions of 2.5 cm covered with paraffin, to losses and gains calculations in isoelement alteration. These cubes were weighed in air and in water, as proposed by Millot and Bonifas (1955). After this step, calculations of geochemical losses and gains were made through the mass balance formula proposed by Millot and Bonifas (1955).

RESULTS

Macromorphological aspects

All the soils described are deep and have similar morphology (Table 1). They are composed of the A, Bw, and C horizons, with or without transitional horizons between them. An exception occurs in Ferralsol 1, which has not reached the C horizon. The A and B horizons have a dark brown (7.5YR 3/4) and a reddish-yellow (7.5YR 6/8) color, respectively. All the horizons contain bauxite fragments that are larger, more angular, and more abundant with depth (Figure 2). In the Ferralsol 1, 2, and 3 profiles, fragment sizes range from 7.9 to 13.7 cm in the C horizons, from 0.25 to 3.5 cm in the Bw horizons, and from 0.2 to 1.7 cm in the A horizons. In general, the fragments are yellowish red (5YR 4/6) to reddish yellow (7.5YR 7/6).

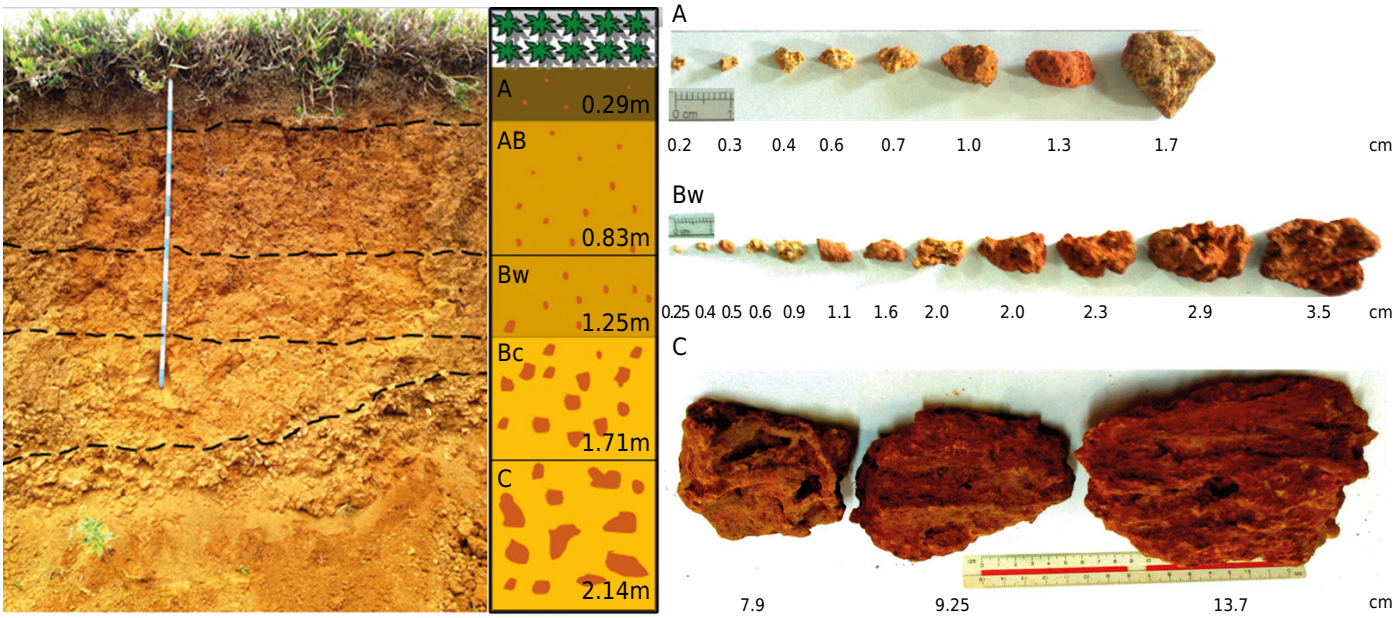

Figure 2. The L3 profile with pedological horizons A, AB, Bw, BC, and C delimited. Bauxite fragments with variable size are visible to the right.

The aggregates in the A horizons occur as small (1 mm) to intermediate (4 mm) granules, which exhibit weak to strong development. In the Bw horizons, the aggregates have intermediate (15 mm) to large (30 mm) size and occur in subangular blocks with a weak degree of development. Bauxite fragments were found inside the aggregates of the Bw and C horizons. In the C horizons, the bauxite fragments are separated by the soil matrix between the subangular blocks (7 mm).

The macromorphological aspects of the soil profiles analyzed are very similar, showing, from bottom to top, an increase in the degree of disaggregation marked by the decrease in the size of bauxite fragments in a typical fining-upward process.

Soil physical and chemical properties

The clay fraction is predominant in all the profiles (Table 1). The A horizons have clay texture and the Bw horizons are clayey to very clayey, with more than 600 g kg^{-1} of clay. In the C horizons, the matrices that surround the bauxite fragments are also clayey to very clayey. The silt/clay relationship shows a slight increase in silt content toward the top of the profiles, which could suggest the progressive weathering of minerals from the sand fraction to the silt fraction, such as quartz and opaque minerals (anatase).

The bulk density (BD) of bauxite fragments in the C horizons of the Ferralsol 2 and Ferralsol 3 profiles and in the undisturbed samples in the Bw horizons of the Ferralsol 1 and Ferralsol 3 profiles have very close average values: 1.01 Mg m^{-3} for fragments and 1.02 Mg m^{-3} near the ground (Table 1).

The mass balance in Ferralsol 2 profile (Table 2) shows the expressive gains of Si and losses of Al and Fe in all horizons. The losses of Na, K, Mg, P, and Mn are related to a greater mobility of these chemical elements.

All the profiles show acidic conditions, with pH(H_2O) between 4.4 and 4.7 (Table 3). The sum of bases (SB), effective CEC, and potential CEC are very low, which implies very leached soils. Base saturation (V) is always under 50 % (Table 3), which characterizes the three profiles as dystrophic. The content of Al^{3+} in the exchange complex is not high (an elevated value is found in the A horizon of Ferralsol 3 = 1.4 $cmol_c$ kg^{-1}) and reaches zero in some horizons. However, Al^{3+} corresponds to more than 80 % of CEC. The total organic carbon (TOC) increases towards the surface (Table 3).

Table 1. Soil morphological and physical properties of the three studied profiles (Ferralsols 1, 2, and 3)

Hor[1]	Layer	Particle size					Silt/ clay ratio	Textural class	Wet color	Consistency			Structure	Bulk density
		>2 mm	<2 mm							Dry	Moist	Plasticity		
		Gravel	Coarse sand	Fine sand	Silt	Clay								
	m	%	g kg^{-1}											mg m^{-3}
Ferralsol 1														
A	0.00-0.32	1.91	330	90	90	490	0.18	Clay	Dark brown (7.5YR 3/4)	Slightly hard	Friable	Slightly plastic	Granular weak fine to medium	1.03
Bw1	0.32-0.94	1.57	250	90	70	590	0.12	Clay	Reddish yellow (7.5YR 6/8)	Slightly hard	Friable	Plastic	Angular blocks weak medium to coarse	1.02
Bw2	0.94-2.00^{+}	6.62	270	50	60	620	0.10	Very clayey	Reddish yellow (7.5YR 6/8)	Slightly hard	Friable	Plastic	Angular blocks weak medium to coarse	1.02
Ferralsol 2														
A	0.00-0.55	5.03	270	100	100	530	0.19	Clay	Dark brown (7.5YR 3/4)	Slightly hard	Friable	Slightly plastic	Subangular blocks moderate fine to medium	1.03
Bw1	0.55-0.96	7.19	210	130	110	550	0.20	Clay	Reddish yellow (7.5YR 6/8)	Slightly hard	Friable	Slightly plastic	Subangular blocks moderate fine to medium	1.02
Bw2	0.96-1.36	4.08	210	60	100	630	0.16	Very clayey	Reddish yellow (7.5YR 6/8)	Slightly hard	Friable	Slightly plastic	Subangular blocks moderate medium to coarse	1.02
C	0.36-1.62^{+}	30.36	230	30	160	580	0.28	Clay (matrix)	Reddish yellow (7.5YR 6/8) (matrix) and yellowish red (5YR 4/6) (bauxite fragments)	Slightly hard (matrix)	Friable (matrix)	Slightly plastic (matrix)	Bauxite fragments coarse enveloped by clay matrix with subangular blocks weak	1.01
Ferralsol 3														
A	0.00-0.29	4.24	310	50	120	520	0.23	Clay	Dark brown (7.5YR 3/4)	Slightly hard	Firm	Slightly plastic	Granular strong fine to medium	-
AB	0.29-0.83	3.74	240	50	80	630	0.13	Very Clayey	Dark brown (7.5YR 3/4)	Slightly hard	Firm	Slightly plastic	Subangular blocks moderate medium to coarse	1.01
Bw	0.83-1.25	6.58	250	40	60	650	0.09	Very clayey	Reddish yellow (7.5YR 6/8)	Slightly hard	Firm	Slightly plastic	Angular blocks weak medium to coarse	1.02
BC	1.25-1.71	7.34	240	40	80	640	0.13	Very clayey (matrix)	Reddish yellow (7.5YR 6/8) (matrix and bauxite fragments)	Slightly hard (matrix)	Firm (matrix)	Plastic (matrix)	Bauxite fragments medium to coarse enveloped by clay matrix with subangular blocks weak fine	-
C	1.71-2.14	-	-	-	-		-	-	Yellowish red (5YR 4/6)	-	-	-	Bauxite fragments coarse	1.01

Hor[1]: horizon. Sand, silt and clay determined by Pipette method; and bulk density determined by Paraffin method.

Table 2. Chemical composition and isoelement titanium (Iso-Ti) mass balance of Ferralsol 2 profile

	Chemical composition					Iso-Ti mass balance			
	C(Bx)	C(Matrix)	Bw2	Bw1	A	C(Bx)-C(matrix Bx)	C(Bx)-Bw2	C(Bx)-Bw1	C(Bx)-A
BD (mg m^{-3})	1.01	1.02	1.02	1.02	1.03				
SiO_2 (%)	4.83	19.6	19.0	19.1	19.9	224	222	215	232
Al_2O_3 (%)	44.4	32	32.2	32.1	31.6	-42	-41	-42	-43
Fe_2O_3 (%)	20.4	22.3	22.3	22.2	21.0	-13	-11	-13	-17
TiO_2 (%)	2.59	3.29	3.19	3.26	3.29	1	1	0	2
Na_2O (%)	0.1	0.1	0.1	0.1	0.1	-20	-18	-20	-19
K_2O (%)	0.01	0.01	0.01	0.01	0.02	-20	-18	-20	61
CaO (%)	0.02	0.03	0.03	0.03	0.03	20	23	20	21
MgO (%)	0.16	0.14	0.15	0.13	0.12	-30	-23	-35	-40
P_2O_5 (%)	0.383	0.284	0.259	0.248	0.251	-41	-45	-48	-47
MnO (%)	0.03	0.02	0.03	0.03	0.03	-47	-18	-20	-19

BD: bulk density; Bx: bauxite fragment. The negative values indicate loss of elements and positive values gain of elements (Millot and Bonifas,1955). Bulk density and Iso-Ti mass balance (Millot and Bonifas, 1955). Chemical Composition: XRF analyses.

Considering base saturation (V) of less than 65 % in the A horizon and the degree of medium to strong structure, soil color with value of 3, organic matter content higher than 6 g kg^{-1}, and thickness of the A horizon greater than 0.25 m, this soil has a prominent A horizon (Santos et al., 2013). The total chemical composition according to XRF shows high levels of Al_2O_3 in both bauxite fragment samples from the C horizons in the Ferralsol 2 and 3 profiles (Table 4). The Al_2O_3 content in the fragments of the horizons is always greater that 40 %, whereas the content in the matrix that surrounds these fragments, which constitutes the main component of the A and B soil horizons, ranges from 30 to 32 %. The SiO_2 content is higher in the soil clay matrix than in the bauxite fragments, and the Fe_2O_3 contents are similar, except for the fragment of the Ferralsol 3 profile, in which the Fe_2O_3 content is lower than in the Ferralsol 2 profile. This difference in Fe_2O_3 content could be attributed to higher concentrations of Fe and Mg oxides in the mafic enclaves in charnockite rock, from which the bauxite is originated (Soares, 2013; Soares et al., 2014). Considering these tropical soils, the TiO_2 content can be considered high, accompanying Al. Other oxides (CaO, MgO, Na_2O, K_2O, and MnO) were very rare, sometimes below the detection limit, even in the C horizons.

Table 3. Chemical properties of the three studied profiles (Ferralsols 1, 2 and 3)

Horizon	Layer	pH(H_2O)	K^+	Ca^{2+}	Mg^{2+}	Al^{3+}	H+Al	SB	CEC(t)	CEC(T)	V	m	TOC
	m		cmol$_c$ dm^{-3}								%		g kg^{-1}
Ferralsol 1													
A	0.00-0.32	4.7	0.04	0.1	0.0	0.8	8.42	0.14	0.94	8.56	2	85	22.39
Bw1	0.32-0.94	4.4	0.01	0.1	0.0	0.5	6.27	0.11	0.61	6.38	2	82	14.58
Bw2	0.94-2.00$^+$	4.7	0.01	0.1	0.0	0.0	2.64	0.11	0.11	2.75	4	0	8.99
Ferralsol 2													
A	0.00-0.55	4.5	0.03	0.1	0.0	1.0	8.42	0.13	1.13	8.55	2	88	23.14
Bw1	0.55-0.96	4.7	0.02	0.1	0.0	0.5	8.25	0.12	0.62	8.37	1	81	19.43
Bw2	0.96-1.36	4.4	0.01	0.1	0.0	0.8	8.42	0.11	0.91	8.53	1	88	19.43
C (matriz)	0.36-1.62$^+$	4.3	0.01	0.1	0.0	0.9	9.08	0.11	1.01	9.19	1	89	18.67
Ferralsol 3													
A	0.00-0.29	4.5	0.06	0.1	0.1	1.4	10.4	0.26	1.66	10.66	2	84	26.33
AB	0.29-0.83	4.5	0.01	0.1	0.0	0.5	6.27	0.11	0.61	6.38	2	82	13.92
Bw	0.83-1.25	4.6	0.00	0.1	0.0	0.0	2.97	0.10	0.10	3.07	3	0	11.42
BC (matriz)	1.25-1.71	4.5	0.00	0.1	0.0	0.0	2.48	0.10	0.10	2.58	4	0	8.41

pH(H_2O): pH in water-saturated soil paste (1:2.5); K^{+1} (Mehlich 1); Ca^{2+}, Mg^{2+}, and Al^{3+} (KCl 1 mol L^{-1}); H+Al (Calcium acetate 0.5 mol L^{-1} - pH 7.0); SB: sum of bases; CEC(t): effective cation exchange capacity; CEC(T): potential cation exchange capacity (at pH 7.0); V: bases saturation; m: aluminum saturation; TOC: total organic carbon (Yeomans and Bremner, 1988).

Table 4. Total chemical composition obtained by XRF, expressed in percentage of oxides, of the three studied profiles (Ferralsols 1, 2, and 3)

	Horizon	SiO_2	Al_2O_3	Fe_2O_3	CaO	MgO	TiO_2	P_2O_5	Na_2O	K_2O	MnO	LOI
		%										
Ferralsol 1	A*	18.7	32.3	20.4	0.03	0.16	4.22	0.185	<0.1	0.01	0.03	23.02
	Bw1*	23.2	32.3	19.6	0.03	<0.10	4.01	0.187	<0.1	0.01	0.03	20.09
	Bw2*	18.0	35.8	20.9	0.02	0.15	4.16	0.211	<0.1	0.01	0.03	20.23
Ferralsol 2	A*	19.9	31.6	21.0	0.03	0.12	3.29	0.251	<0.1	0.02	0.03	23.09
	Bw1*	19.1	32.1	22.2	0.03	0.13	3.26	0.248	<0.1	0.01	0.03	22.45
	Bw2*	19.0	32.2	22.3	0.03	0.15	3.19	0.259	<0.1	<0.01	0.03	21.68
	C (matrix)*	19.6	32.0	22.3	0.03	0.14	3.29	0.284	<0.1	0.01	0.02	21.25
	C (bauxite fragment)	4.83	44.4	20.4	0.02	0.16	2.59	0.383	<0.1	<0.01	0.03	26.34
Ferralsol 3	A*	21.8	30.4	18.8	0.03	0.14	3.65	0.210	<0.1	0.02	0.03	23.82
	ABw*	21.1	33.5	19.5	0.03	0.16	3.40	0.216	<0.1	0.01	0.03	20.63
	Bw*	19.7	35.7	19.9	0.02	0.16	3.23	0.239	<0.1	0.02	0.02	20.26
	BwC*	19.4	36.1	20.0	0.03	0.14	3.21	0.226	<0.1	0.01	0.02	19.77
	C (bauxite fragment)	13.0	49.6	9.37	0.03	0.17	1.15	0.164	<0.1	<0.01	<0.01	26.29

*sand, silt, and clay fractions. LOI: loss on ignition. The SiO_2, Al_2O_3, Fe_2O_3, CaO, MgO, TiO_2, P_2O_5, Na_2O, K_2O, and MnO were determined by the alkaline fusion method.

Soil mineralogy

The XRD analysis revealed the presence of gibbsite, quartz, goethite, kaolinite, hematite, and anatase in the A, Bw, and C matrix in all the profiles (Figure 3). The bauxite fragments also had gibbsite, quartz, hematite, and goethite (C horizon) (Figure 3). Kaolinite and anatase were only identified in some bauxite fragments. The reflection intensity of gibbsite decreased from the bauxite fragments to the soil, and a significant increase in the quartz reflection occurred.

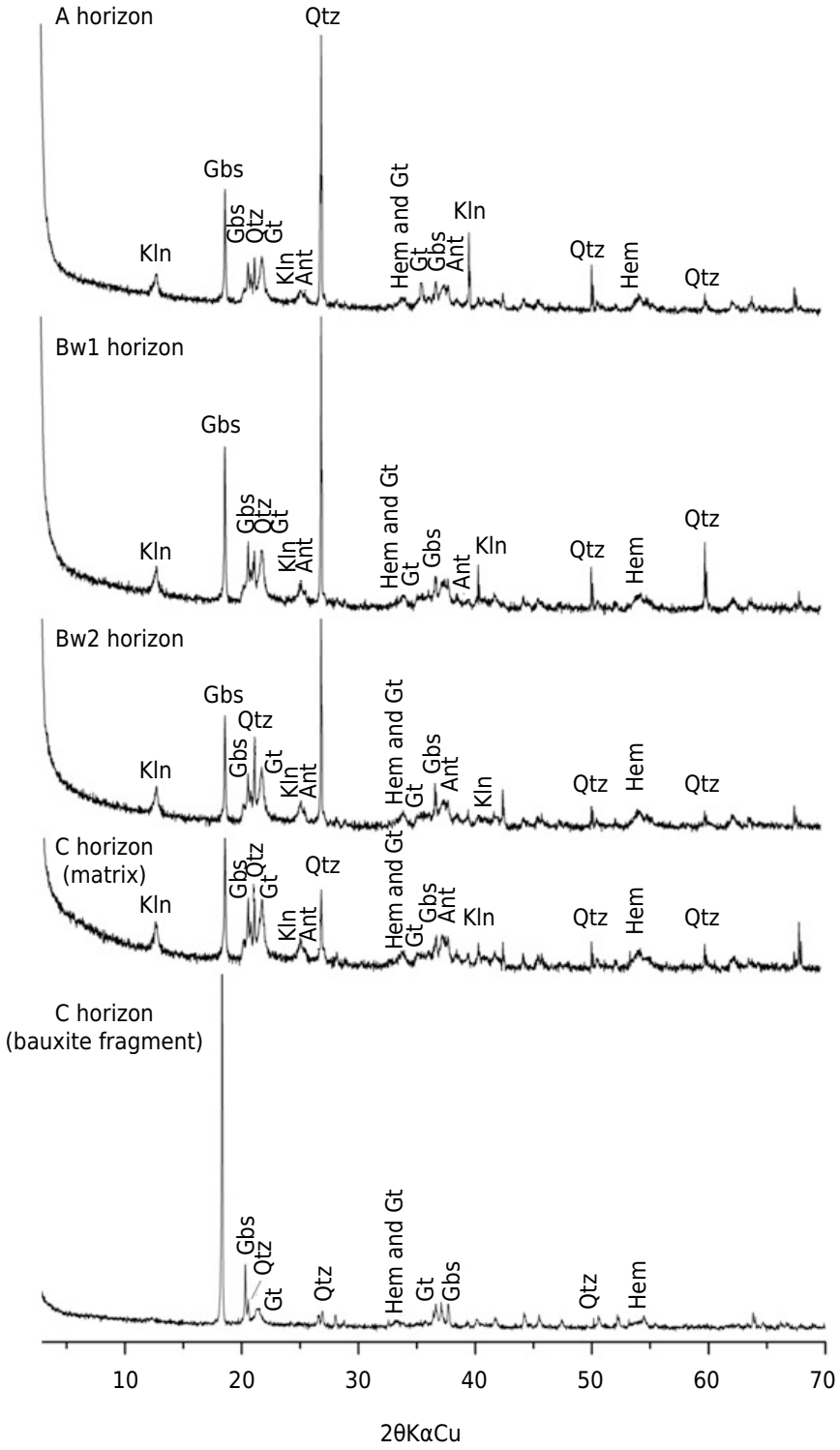

Figure 3. X-ray diffractograms, which show the mineralogical composition of the A, Bw, and C horizons and the bauxite fragments in the C horizon.

Soil micropedology

The bauxite fragments in the C horizon are heterogeneous, with greater and lesser degrees of degradation. The less degraded regions consist of gibbsitic micromass with crystallitic b-fabric (Figures 4a and 4b). Some fragments show the same band orientation of the bauxite source material (charnockite). These fragments represent the isalteritic levels that were described by Soares et al. (2014), including the presence of ferromagnesian alteromorphs (Figure 4c). The more degraded fragments in the C horizon consist of gibbsite-kaolinitic micromass with undifferentiated b-fabric and a reddish-yellow color (7.5YR 6/8) (Figures 4d, 4e, and 4f). The matrix that envelopes the bauxite fragments contains coarse quartz, opaque minerals, and rare zircon crystals (Figure 4f). The quartz crystals are anhedral and angular, with undulose extinction, and fall within the coarse sand fraction. The opaque minerals and zircon crystals constitute 5 % of the modal composition and occur in the thin sand fraction. The relative distribution between the coarse and thin grains is of porphyric type. The predominant microstructure is of massive type (Figure 4g), along with the occurrence of subrounded blocks (Figure 4h). Voids are present, mainly in the form of vugs that reach 3.5 mm (major axis length), along with vesicles (0.25 mm).

Microchemical mapping of the contact between the more and less degraded regions of bauxite fragments show an increase in silica and a decrease in Al towards the more degraded portions (Figure 5a). This relationship is also observed through a punctual (Figure 5b) and linear (Figure 5c) chemical composition, which shows that Si displays a high peak in the more degraded portions while Al is higher than Si in the less degraded portions.

Micromorphologically, the Bw horizons are very similar in all profiles. The microstructure is formed by accommodated to partly accommodated subangular blocks with moderate spacing and development (Figures 6a and 6b). Microaggregated microstructure that consists of strongly separated, rounded peds also occurs (Figures 6b, 6c, and 6d). The predominant voids are fissures, compound packing in the block domains, and complex packing in the microaggregate domain. The coarse material in the s-matrix consists of quartz grains in the fine sand fraction (100 µm) with undulose extinction, angular to subangular form (Figures 6d and 6e), and opaque crystals in the medium sand fraction (150 µm). Together, the coarse grains constitute approximately 30 % of the matrix background. Some quartz crystals have fractures that are filled by micromass. Based on the Bw horizons (Bw2), the bauxite fragments reach 450 µm and exhibit quartz ribbons that are similar to those in the C horizons and isalteritic bauxite, as described by Soares et al. (2014) (Figure 6f).

In the upper portion of the Bw horizons, the fragments are rare and smaller, ranging from 2.5 to 4.0 mm along their major axis length. In all, these fragments do not make up more that 0.5 % of the total thin sections and may be included as coarse material (Stoops, 2003).

The Bw horizons have yellowish-red micromass (7.5YR 6/8) with dotted-mottled b-fabric. Two relative distributions occur in the s-matrix. First is a porphyric type distribution, in which quartz crystals are immersed in the fine material inside the aggregates (Figure 6e). Second is an enaulic type distribution, which exhibits separation between fine and coarse material; the fine material appears as microaggregates and dissociated quartz crystals (Figures 6d, 6e, and 6h). In this second case, coal fragments are commonly present in the micromass as organic constituents.

The most common pedofeatures are infillings (Figure 6g) and, secondarily, nodules (Figures 6a and 6h) and coatings. The infillings form as a result of biological activity and highlight the role of biological activity in the structure and porosity of the soils analyzed. The nodules have dark-red color and sizes from 1.0 to 2.5 mm, constituting approximately 0.5 % of the composition of the thin section. These nodules are classified as typical nodules. There are also organic nodules. Coatings are uncommon, constituting only small portions of the thin section, and they are classified as typical coatings.

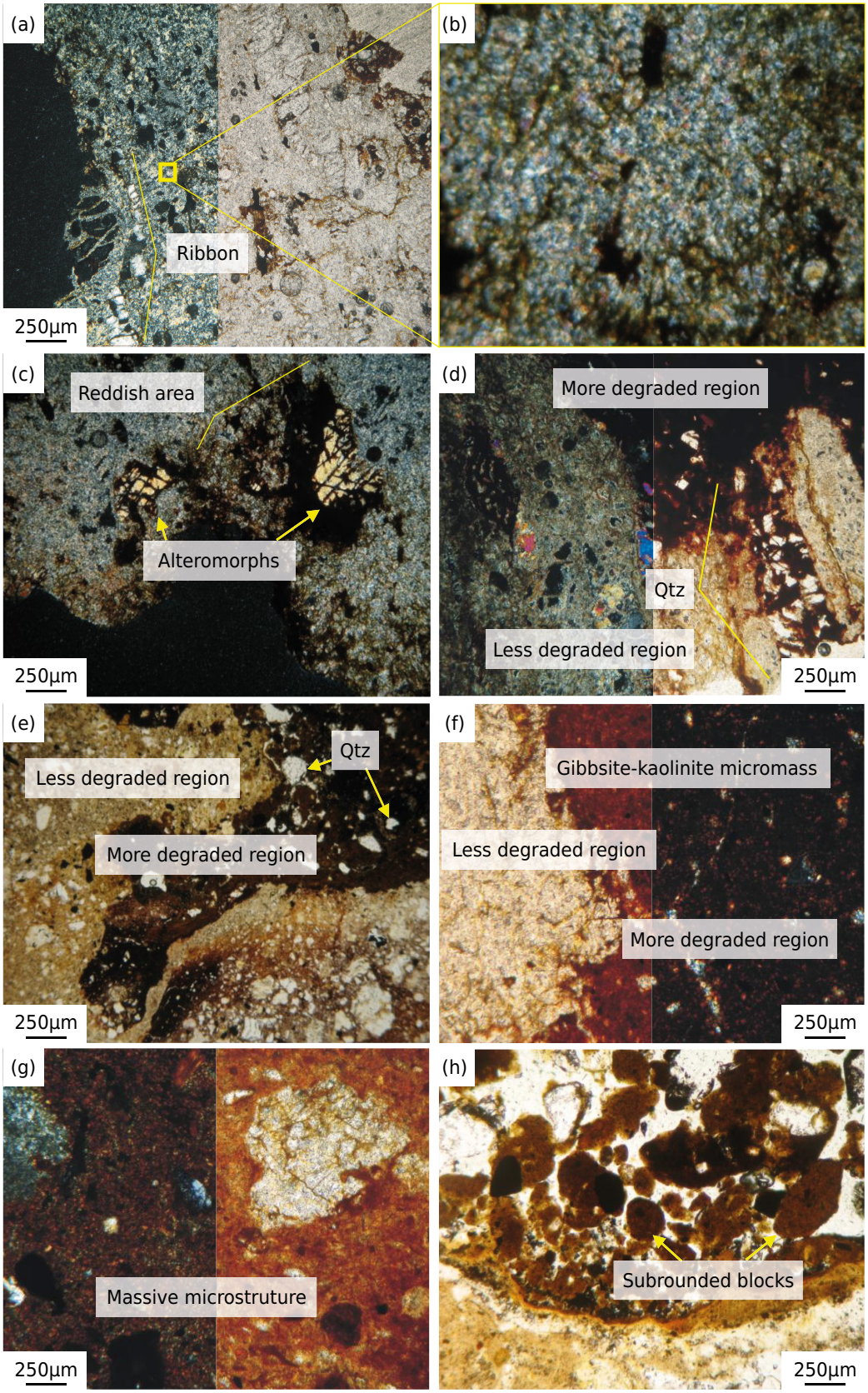

Figure 4. Photomicrograph of bauxite fragments. PPL: plane polarized light; XPL: crossed polarized light; Qz: quartz. (a) Less degraded bauxite fragment with preserved isalteritic structure and quartz ribbons. The micrograph on the right was taken under XPL and on the left under PPL. (b) Gibbsite micromass with crystalline b-fabric. (c) Bauxite fragment with a reddish region indicating the precipitation of iron oxide and the presence of ferromagnesian alteromorphs. (d), (e), and (f) Bauxite fragment with regions with varying degradation. The more degraded region consists of reddish-yellow gibbsite-kaolinite micromass, and the less degraded region consists of gibbsite micromass with crystalline b-fabric. Photomicrograph (d) shows the right side under XPL and the left side under PPL. (g) Massive microstructure, taken under XPL on the right and PPL on the left. (h) Microstructure with subrounded blocks.

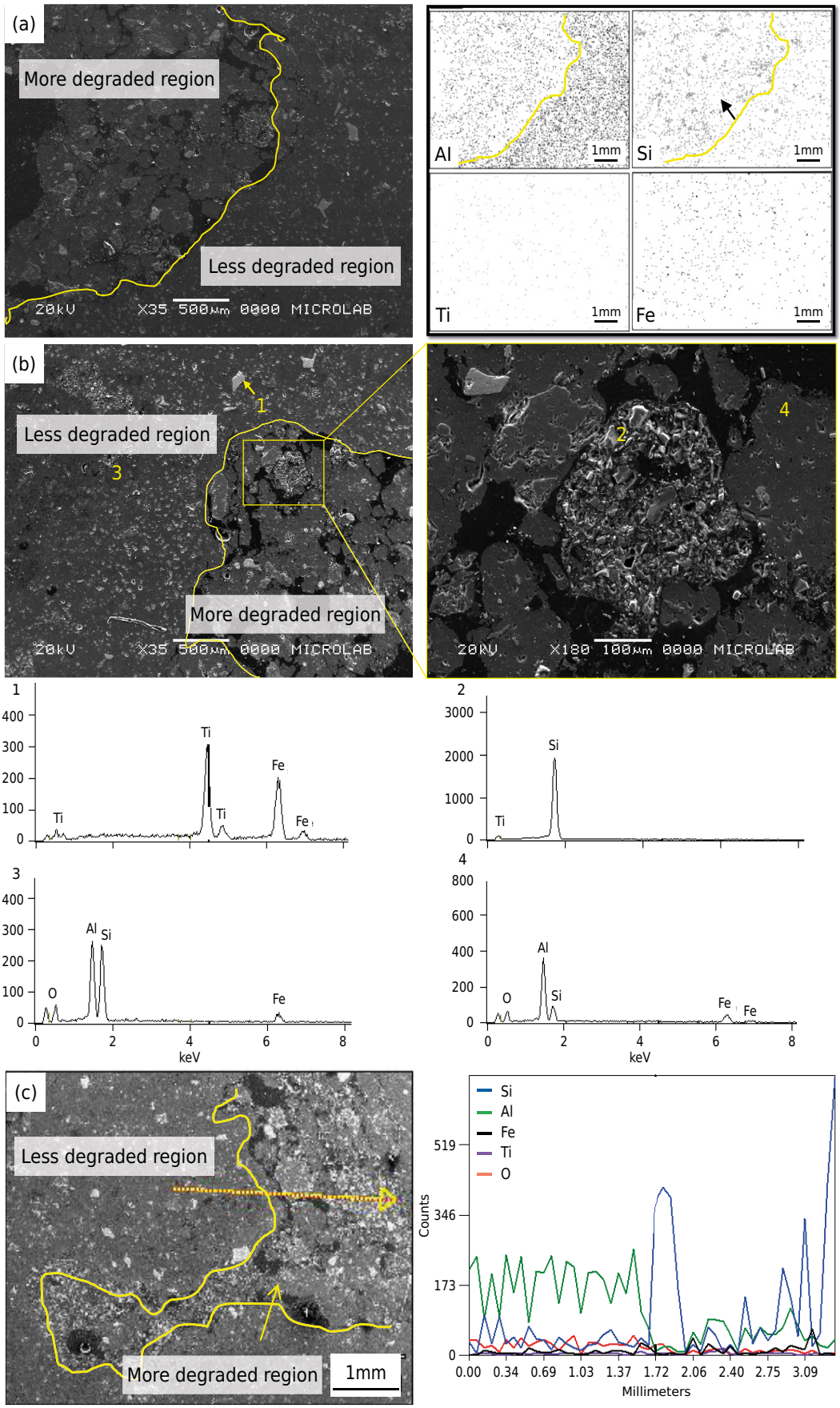

Figure 5. Scanning electron microscopy photomicrograph and microchemical map that shows the Si accumulation in the more degraded portions of bauxite. (a) The arrow indicates the direction of Si accumulation in microchemical mapping. (b) Microchemical analysis by Electron Dispersive X-ray (EDS), which indicates the chemical compositions of different regions of the bauxite. (c) Linear microchemical analysis, which indicates an increase in Si in the more degraded portions of the bauxite. The yellow arrow indicates the direction of enrichment in Si.

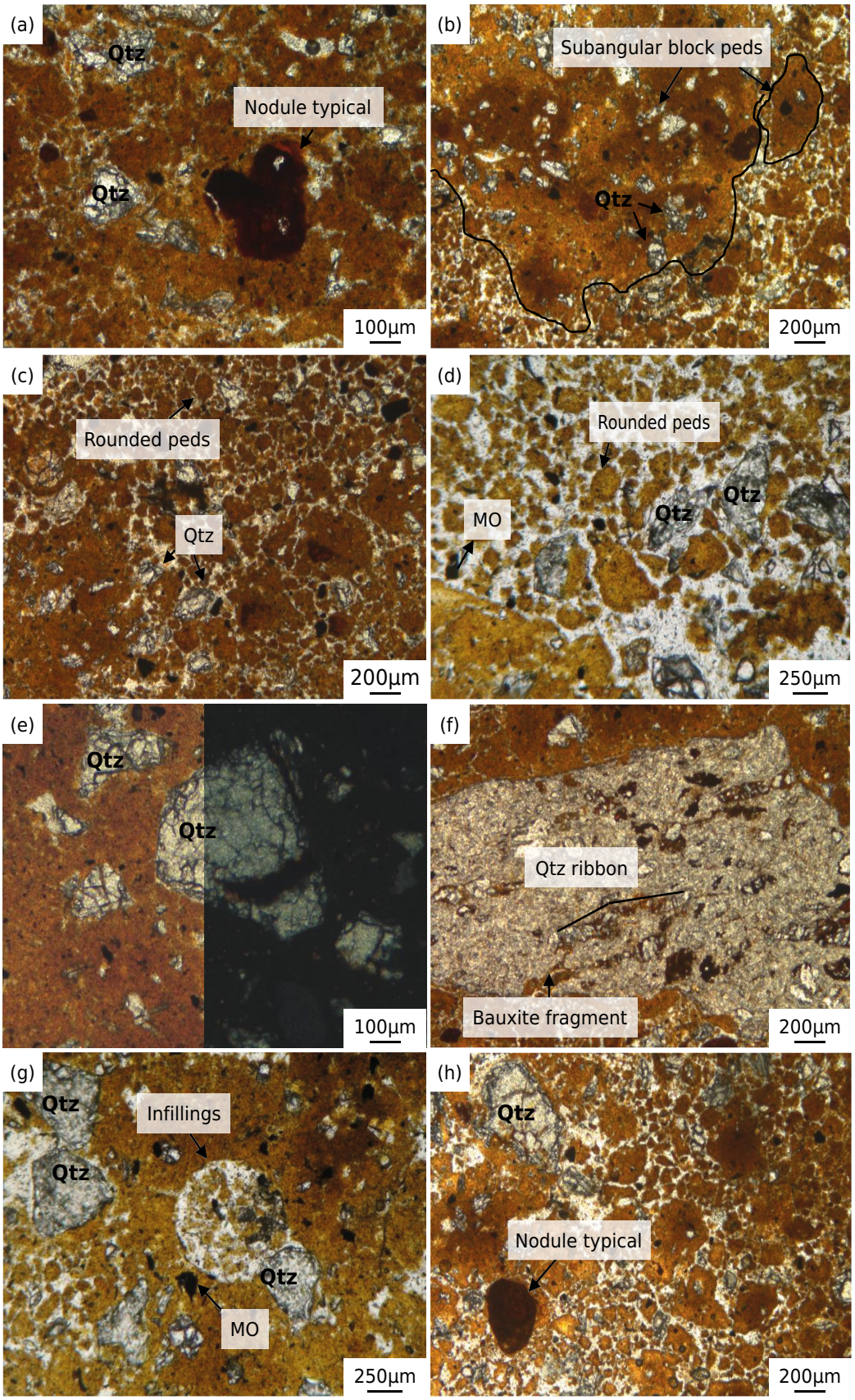

Figure 6. Photomicrograph of the Bw horizon. PPL: plane polarized light; XPL: crossed polarized light; Qz: quartz; OM: organic matter. (a) Subangular blocky microstructure. (b) Microaggregate microstructure with strongly separated rounded peds. (c) Microaggregate microstructure with strongly separated rounded peds and angular and subangular quartz. (d) Enaulic coarse/fine (c/f) related distribution with quartz grains that are separated in fine material. (e) Porphyritic c/f related distribution with angular quartz. The right side of the photomicrograph was taken under PPL and the left under XPL. (f) Bauxite fragment with ribbon. (h) Oxi-hydroxide typical nodules with an enaulic c/f related distribution.

DISCUSSION

Aluminous duricrust as soil parent material

The morphological properties (macro and micro), including physical, chemical, and mineralogical, indicate that the three profiles analyzed are *Latossolo Amarelo Distrófico típico* (Santos et al., 2013a), which corresponds to Xantic Ferralsols in the FAO System (Soil Survey Staff, 2014). The parent material of these Ferralsols is bauxite and not the rock that is found in the area, specifically, charno-enderbitic gneiss with mafic inclusions (Horn et al., 2007; Novo et al., 2011; Soares et al., 2014).

The morphology of the horizons and the presence of bauxite fragments in the base profile suggest that the solum (A + Bw) originated from the degradation of these fragments. In the A and Bw horizons, the fragments are smaller and more degraded, representing lithorelict nodules. Even the presence of fragments indicates the physical degradation of an ancient level of massive bauxite. This level was described by Soares (2013) and exists below the fragments, completing a lateritic profile (Nahon and Tardy, 1992).

In addition to the macromorphological aspects, analytical results confirm the genetic relationship between aluminous duricrust and the soil. These soils contain the same minerals that are present in the bauxite, along with kaolinite. No record exists of primary minerals such as feldspar and iron and magnesium oxides as those that occur in the charno-enderbite gneisses of the area; instead, only those minerals that are produced by weathering (gibbsite, goethite, hematite, etc.) or residual alterations, such as quartz, are present in the bauxite.

Weathered gneiss can form increasing amounts of clay soils and lower the silt/clay ratio. However, an increase in silt content is observed in the soil analyzed. Bauxite immediately produces a very clay-like soil. To the extent that the soil evolves, the mineral sand fraction, such as quartz, is mechanically degraded by bioturbation to the silt fraction (Schaefer, 2001). Thus, the soil becomes more clayey with increasing weathering when soil origin is related to degradation of the aluminous duricrust. At the microscopic level, this fragmentation of quartz grains by bioturbation is even more evident (Figure 6d).

The total chemical composition does not indicate Ca or K content that represent alteration of minerals such as plagioclases and orthoclases that are present in charno-enderbite (Horn et al., 2007; Novo et al., 2011; Soares et al., 2014). This observation occurs even at the level of alterite, the C horizon, where some amounts of more mobile elements can be found. Even so, soils that originate directly from crystalline rock have base saturation that ranges between 10 and 30 %. In the case of soils, the highest value was 4 %; the nutrient availability was extremely low. These low values also occur in bauxite, suggesting that bauxite would be more adept at generating soils with such chemical properties. This feature occurs in aluminous pedogenesis, the formation of a soil from a pre-weathered material.

Resilication process and its indicators

The transformation of duricrust in soils is a topic of interest for understanding the evolution of mantles in the tropics (Boulangé and Carvalho, 1989). In the specific case of aluminous duricrust, the bauxite and various deposits that are studied throughout the world present features and materials that have been associated with such processes. In most of them, the principal mechanism is exposure to silica-rich solutions, which facilitate the resilication of bauxite (Lacroix, 1913; Harrison, 1934; Lacroix, 1934; Van der Marel, 1960; Keller and Clarke, 1984) or kaolinitization (Dangić, 1985), in which the silica source would be the *in situ* materials. The enrichment of Si in the upper horizons could also be by entry and accumulation of chemically mature debris of allochthonous origin, such as eolian influx described by Brimhall et al. (1991).

The presence of clay horizons whose genesis can be attributed to the resilication of old bauxitic levels has been recognized in several deposits in Brazil (Boulangé and Carvalho, 1989; Lucas, 1997; Varajão et al., 1989, 1990; Horbe and Costa, 1999; Oliveira et al., 2013b). In the Amazon, for example, the clay layer on top of many deposits, such as Porto de Trombetas, Juruti, Rio Capim, and Paragominas, was described as homogeneous, without stratification, and eminently kaolinitic. This layer also occurs at the base of the profiles of the Porto Trombetas, Juruti, and Rio Capim deposits. Several aspects emphasize their autochthonous origin from the transformation of bauxite, and prominent among them are the following: i) the presence of angular grains of quartz that are very fractured and filled with clay matrix material, ii) the presence of gibbsite nodules with a gradual transition to the matrix, iii) the presence of non-ferruginous zones and/or ferruginous nodules that indicate iron remobilization, and iv) enrichment in Ti and Zr (Boulangé and Carvalho; 1989).

The soil profiles that were analyzed in this study had aspects that suggest an input of silica of unknown origin that participates in their formation process. These indicators are related to mineralogical, geochemical, and micromorphological transformations.

The mineralogical indicators are related to a decrease in gibbsite and an increase in kaolinite, which is reflected in the intensity of the peaks in the X-ray diffraction patterns. Mineralogical studies have shown that when an increase in silica activity in the solution is accompanied by decreased pH, gibbsite is unstable and tends to turn into kaolinite (Lindsay, 1979). The kaolinite that forms is small (<1 μm), with irregular shapes and structural defects (Singh and Gilkes, 1992; Varajão et al., 2001; Oliveira et al., 2013a). The poorly defined XRD peaks (Figure 3) in the 20-27° 2θ range reflect the morphological and crystalochemical features of the kaolinite crystals. Additionally, the decrease in gibbsite in the matrix leads to a relative concentration of quartz, which shows the most intense diffraction peaks.

Geochemical indicators are related to the behavior of Al, Si, Fe, and Ti in terms of both the total contents that are adsorbed into the exchange complex between colloidal particles and the soil solution. For the total concentration, the iso-Ti mass balance profile in Ferralsol 2 (as an example) shows the gain and loss in the resilication process (Table 2). In comparison, enrichment in silica is present in all horizons. The most important losses are aluminum and iron, which are both associated with the decomposition of minerals such as gibbsite and goethite. In the case of goethite, iron remobilization tends to form the ferruginous nodules that were identified in the thin sections.

The results show that the 'm' index in the profiles tends towards zero in the lower horizons and towards more than 80 % in the upper horizons. This behavior suggests that the Al is in the form of gibbsite at the base of the profile. As gibbsite destabilizes, the free Al^{3+} increases in the soil solution, suggesting an in situ epigenetic replacement of alumina in gibbsite by dissolved silica, similar to the process proposed by Dangić (1985) and Liu et al. (2010). Thus, the release of Al^{3+} is a direct consequence of the resilication process.

The observed organic matter content (including depth) is higher than what is expected for very weathered tropical soils (Sombroek et al., 1993; Tiessen et al., 1994). The presence of high organic C in Ferralsols is understood as an important paleoenvironmental indicator, a product of hot and humid weather (Queiroz Neto and Castro, 1974; Lepsch and Buol, 1988; Ker, 1997; Buol and Eswaran, 1999; Calegari, 2008; Marques, 2009). This behavior corroborates that physicochemical changes in the weathering system must occur to facilitate the resilication of bauxite on the surface. These changes will destabilize gibbsite and should provide a silica source for the neoformation of kaolinite. The ideal conditions for these changes occur from vegetation growth on the surface, which is usually associated with the transition from a dry climate to a more humid climate. During previous dry weather, erosion on the unprotected surface could expose the bauxite. With the transition to a humid climate, the growth of vegetation

starts to mechanically break up the massive bauxite. The decomposition of the organic matter lowers the pH and reintroduces many chemical compounds, such as silicon. Little is known about the precise source of this silicon, although a relationship to the decomposition of Si-phytoliths may exist. However, the role of vegetation in biogeochemical cycling is definitely important (Alexandre et al., 1997). This effect can also influence the type of charge that is predominant in clays. With the transformation of gibbsite into kaolinite, the soil tends to have increasingly negative charges, leaving it electropositive. This behavior is opposite to what is expected for the developed soils of quartz-feldspathic rocks.

Micromorphological indicators of the resilication process are related to the emergence of a new set of microstructures and pedofeatures. These microstructures are formed as features that are associated with bauxite disappear. The first feature is the formation of relict nodules of bauxite (gibbsite). These nodules contain internal microstructure features of the bauxitization process. The internal microstructure features which will cease to exist and will become micromass clay with gibbsite crystals immersed in a kaolinite matrix. The kaolinite in this study coexists with gibbsite nodules, suggesting kaolinite is the product of the in situ epigenetic replacement of alumina in gibbsite by dissolved silica, similar to the process proposed by Dangić (1985) and Liu et al. (2010). Following the formation of this micromass, the aggregation of blocks occurs with a porphyric type structure that is separated by fissure pores that exhibit illuviation features, with micromass as the filling material and not detritus of allochthonous origin. According to Brimhall et al. (1991), the detritus material would be one of the sources of the enrichment in Si, calculated through mass balance. In this study, the iso-Ti mass balance also showed a gain in Si and a loss in Al, but there is no evidence to attribute this enrichment to the illuviation.

An increase in biological colonization occurs because the aggregation of blocks can retain more moisture and is comparatively richer in organic matter than bauxite. With endopedonic fauna now established, bioturbation results in the construction of termitic microaggregates (Schaefer, 2001). These microaggregates represent the opening of porosity and the transition to an enaulic relative distribution. Although not directly related to resilication, the formation of microaggregates is possible only because the degradation of bauxite provides an opportunity for biological colonization.

CONCLUSIONS

The macromorphological, micromorphological, mineralogical, and chemical evidence, such as reduction in the size and quantity of bauxite fragments towards the top of profiles, the increase in kaolinite in the matrix of the horizons with gibbsite nodules immersed in diffuse contact, the high amount of exchangeable aluminum in the solum, the increase in SiO_2 exhibited by the iso-Ti mass balance, and a decrease in Al_2O_3 toward the A horizons in all profiles suggest that the origin of the soil cover is presumably related to the degradation of bauxite and the reintroduction of silica into the system.

The origin of the silica was not directly determined in this study, but it is assumed that it could be from the biogeochemical cycling of vegetation *in situ* and, in some cases, water table fluctuations.

ACKNOWLEDGMENTS

The authors thank the Fundação de Amparo à Pesquisa do Estado de Minas Gerais (Fapemig), the Conselho Nacional de Desenvolvimento Científico Tecnológico (CNPq), and the coordinators and staff of the X-ray Diffraction and Geochemical Laboratories of the Geology Department of the Universidade Federal de Ouro Preto (Degeo/UFOP).

REFERENCES

Aleva GJJ. The buried bauxite deposit of Onverdacht, Surinam, South America. Geol Mijnbouw. 1965;44:45-58.

Alexandre A, Meunier JD, Lézine AM, Vincens A, Schwartz D. Phytoliths: indicators of grassland dynamics during the late Holocene in intertropical Africa. Palaeogeogr Palaeoclimatol Palaeoecol. 1997;136:213-29. https://doi.org/10.1016/S0031-0182(97)00089-8

Beissner H, Carvalho A, Lopes LM, Valeton I. The Cataguases bauxite deposit. In: Carvalho A, Boulangé B, Melfi AJ, Lucas Y, editors. Brazilian bauxites. São Paulo-Paris: USP/Fapesp/Orstom; 1997. p.195-208.

Bocquier G, Boulangé B, Ildefonse P, Nahon D, Muller D. Transfers, accumulation modes, mineralogical transformations and complexity of historical development profiles. In: Proceedings of 2nd International Seminar on Laterization; 1982; São Paulo. São Paulo: 1982. p.331-7.

Boulangé B. Les formations bauxitiques latkntiques de Côte d'Ivoire. Les facies, leur transformation, leur distribution et l'évolution du modelt. Trav Docum. 1984;175:341.

Boulangé B, Bocquier G. Le rôle du fer dans la formation des pisolites alumineux au sein des cuirasses bauxitiques latéritiques. Sci Géol. 1983;72:29-36.

Boulangé B, Carvalho A. The genesis and the evolution of the Porto Trombetas bauxite deposits in the Amazon Basin, Brazil. In: Annals of the 6th International Congress for the Study of Bauxite, Alumina and Aluminum (Icsoba). Poços de Caldas: 1989. p.71-79.

Brimhall GH, Christopher JL, Ford C, Bratt J, Taylor G, Warin O. Quantitative geochemical approach to pedogenesis: importance of parent material reduction, volumetric expansion, and eolian influx in laterization. Geoderma. 1991;51:51-91. https://doi.org/10.1016/0016-7061(91)90066-3

Brindley GW, Brown G. Crystal structures of clay minerals and their X-ray identification. London: Mineralogical Society; 1980.

Buol SW, Eswaran H. Oxisols. Adv Agron. 1999;68:151-95. https://doi.org/10.1016/S0065-2113(08)60845-7

Calegari MR. Ocorrência e significado paleoambiental do horizonte A húmico em Latossolos [tese]. Piracicaba: Escola Superior de Agricultura "Luis de Queiroz"; 2008.

Dangić A. Kaolinization of bauxite: a study in the Vlasenica Bauxite area, Yugoslavia. I. Alteration of matrix. Clays Clay Miner. 1985;33:517-24. https://doi.org/10.1346/CCMN.1985.0330606

Donagema GK, Campos DVB, Calderano SB, Teixeira WG, Viana JHM, organizadores. Manual de métodos de análise do solo. 2a ed. rev. Rio de Janeiro: Embrapa Solos; 2011.

Filizola HF, Gomes MA. Coleta e impregnação de solos para análise micromorfológica. Jaguariúna: Embrapa; 2004. (Boletim técnico, 20).

Groke MCT, Melfi AJ, Wackermann JM. Transformações mineralógicas e estruturais ocorridas durante a bauxitização de rochas cristalinas ácidas. Estudo do depósito bauxítico de Mogi das Cruzes, SP. In: Anais do 31º Congresso Brasileiro de Geologia; 1980; Camboriú. Camboriú: Universidade Federal de Santa Catarina; 1980. p.128-35.

Harrison JB. The katamorphism of igneous rocks under humid tropical conditions. Imp Bureau Soil Sci. 1934;71:382-4. https://doi.org/10.1017/S0016756800093614

Horbe AMC, Costa ML. Relações genéticas entre Latossolos e crostas lateríticas aluminosas e alumino-ferruginosas na região de Paragominas, Pará. Rev Bras Geocienc. 1999;29:497-504.

Horn AH, Faria B, Gardini GM, Vasconcellos L, Oliveira ML. Mapa Geológico. Folha Espera Feliz - escala 1:100.000 [mapa]. Minas Gerais, Espírito Santo, Rio de Janeiro: CPRM/UFMG - Programa Geologia do Brasil; 2007.

Keller WD, Clarke Jr OM. Resilication of bauxite at the Alabama Street Mine, Saline County, Arkansas, illustrated by scanning electron micrographs. Clays Clay Miner. 1984; 32:139-46. https://doi.org/10.1346/CCMN.1984.0320208

Ker JC. Latossolos do Brasil: uma revisão. Geonomos. 1997;5:17-40. https://doi.org/10.18285/geonomos.v5i1.187

Lacroix A. Les laterites de Guinée et les produits d'altération qui leur sont associés. Nouv Arch Mus Hist Nat. 1913;5:255-326.

Lacroix A. Introduction aux études minières coloniales. Pub Bur Etudes Géol Min Col. 1934;2:19-47.

Lepsch IF, Buol SW. Oxisoil-landscape relationship in Brazil. In: Annals of 8th International Soil Classification Workshop; 1986; Campinas. Rio de Janeiro: Embrapa, SNLCS; University of Puerto Rico; 1988. p.174-89.

Lindsay WL. Chemical equilibria in soils. New York: John Wiley & Sons; 1979.

Liu X, Wang Q, Deng J, Zhang Q, Sun S, Meng J. Mineralogical and geochemical investigations of the Dajia Salento-type bauxite deposits, western Guangxi, China. J Geochem Explor. 2010;105:137-152.

Lopes LM, Carvalho A. Gênese da bauxita de Miraí, MG. Rev Bras Geocienc. 1990;19:462-9.

Lucas Y, Luizão FJ, Chauvel A, Rouiller J, Nahon D. The relation between biological activity of the rainforest and mineral composition of the soils. Science. 1993;260:521-3. https://doi.org/10.1126/science.260.5107.521

Lucas Y. The bauxite of Juruti. In: Carvalho A, Boulangé B, Melfi AJ, Lucas Y. editors, Brazilian Bauxites. São Paulo: USP/FAPESP/ORSTOM; 1997. p.107-36.

Marques FA. Matéria orgânica de Latossolos com horizonte A húmico [tese]. Piracicaba: Escola superior de agricultura "Luis de Queiroz"; 2009.

Millot G, Bonifas M. Transformations isovolumetriques dans les phenomenes de laterisation et de bauxitisation. Bull Serv Carte Géol d'Alsace Lorraine. 1955;8:3-20.

Munsell. Soil Color Charts. Baltimore: Macbeth Division of Kollmorgen Corporation; 1975

Nahon D, Tardy Y. The ferruginous laterites. In: Butt CRM, Zeegers H, editors. Regolith exploration geochemistry in tropical and subtropical terrains. Amsterdam: Elsevier; 1992. p.41-55.

Novo TA, Noce CM, Pedrosa-Soares AC, Batista GAP. Rochas granulíticas da Suíte Caparaó na região do Pico da Bandeira: embasamento oriental do Orógeno Araçuaí. Geonomos. 2011; 19:70-7. https://doi.org/10.18285/geonomos.v19i2.42

Oliveira FS, Varajão AFDC, Varajão CAC, Boulangé B. A comparison of properties of clay minerals in isalteritic and in degraded facies. Clay Miner. 2013a;48:697-711. https://doi.org/10.1180/claymin.2013.048.5.03

Oliveira FS, Varajão AFDC, Varajão CAC, Boulangé B, Soares CCV. Mineralogical, micromorphological and geochemical evolution of the facies from the bauxite deposit of Barro Alto, Central Brazil. Catena. 2013b;105:29-39. https://doi.org/10.1016/j.catena.2013.01.004

Queiroz Neto JP, Castro SS. Formações superficiais e Latossolos Vermelho-Amarelo Húmico na área de Bragança Paulista. Estado de São Paulo, Brasil. In: Anais do 18º Congresso Brasileiro de Geologia; 1974; Porto Alegre. Porto Alegre: Sociedade Brasileira de Geologia; 1974. p.65-83.

Santos HG, Jacomine PKT, Anjos LHC, Oliveira VA, Oliveira JB, Coelho MR, Lumbreras JF, Cunha TJF. Sistema brasileiro de classificação de solos. 3a ed. Rio de Janeiro: Embrapa Solos; 2013a.

Santos RD, Lemos RC, Santos HG, Ker JC, Anjos LHC, Shimizu SH. Manual de descrição e coleta de solo no campo. 6a ed rev e ampl. Viçosa, MG: Sociedade Brasileira de Ciência do Solo; 2013b.

Schaefer CEGR. Brazilian Latosols and their B horizon microstructure as long-term biotic constructs. Aust J Soil Res. 2001;39:909-26. https://doi.org/10.1071/SR00093

Sigolo JB, Boulangé B. Caracterização das fácies de alteração de uma topo-seqüência no maciço alcalino de Passa Quatro, MG. Rev Bras Geocienc. 1987;17:269-75.

Sigolo JB, Boulangé B. The bauxite deposits of the Passa Quatro alcaline massif, Minas Gerais, Brazil. In: Annals of the 6th International Congress for the Study of Bauxite, Alumina and Aluminum (ICSOBA). Poços de Caldas: 1989. p.159-167.

Singh B, Gilkes RJ. Properties of soil kaolinites from south-western Australia. J Soil Sci. 1992;43:645-67. https://doi.org/10.1111/j.1365-2389.1992.tb00165.x

Soil Survey Staff. Keys to soil taxonomy. 12th ed. Washington, DC: United States Department of Agriculture, Natural Resources Conservation Service; 2014.

Soares CCV. Gênese e evolução mineralógica, micromorfológica e geoquímica da bauxita de Espera Feliz, MG [dissertação]. Ouro Preto: Universidade Federal de Ouro Preto; 2013.

Soares CCV, Varajão AFDC, Varajão CAC, Boulangé B. Mineralogical, micromorphological and geochemical transformations in the initial steps of the weathering process of charnockite from the Caparaó Range, southeastern Brazil. J South Am Earth Sci. 2014;56:30-40. https://doi.org/10.1016/j.jsames.2014.08.005

Sombroek WG, Nachtergaele FO, Hebel A. Amounts, dynamics and sequestering of carbon in tropical and subtropical soils. Ambio. 1993;22:417-26.

Stoops G. Guidelines for analyses and description of soil and regolith thin sections. Madison: Soil Society of America; 2003.

Tewari GP. Occurrence of kaolinite in association with iron-pan. Nature. 1963;198:1019. https://doi.org/10.1038/1981019a0

Tiessen H, Cuevas E, Chacon P. The role of soil organic matter in sustaining soil fertility. Nature. 1994; 371:783-5. https://doi.org/10.1038/371783a0

Van der Marel HW. Quantitative analysis of kaolinite. Silic Ind. 1960;25:23-31 and 76-86.

Varajão CAC, Boulangé B, Carvalho A. The Bauxites of the Quadrilátero Ferrífero, Minas Gerais, Brazil. In: Annals of the 6th International Congress for the Study of Bauxite, Alumina and Aluminum,Travaux du Comitê Internacional Pour L'étude des Bauxites, de L'Alumine et de L'Aluminium (ICSOBA). Poços de Caldas: 1989. p.127-136.

Varajão AFDC, Boulangé B, Melfi AJ. The petrological evolution of the facies in the kaolinite and bauxite deposits of Vargem dos Óculos, Quadrilátero Ferrífero, Minas Gerais, Brazil. In: Annals of the 6th International Congress for the Study of Bauxite, Alumina and Aluminum (ICSOBA). Poços de Caldas: 1989. p.137-146.

Varajão AFDC, Melfi AJ, Boulangé B. Caracterizacão morfológica, mineralógica e química das fácies estruturais da jazida de caulinita de Vargem dos Óculos, Quadrilátero Ferrífero, MG. Rev Bras Geocienc. 1990; 20:75-82.

Varajão AFDC, Gilkes RJ, Hart RD. The relationships between kaolinite crystal properties and the origin of materials for a Brazilian kaolin deposit. Clays Clay Miner. 2001;49:44-59.

Valenton I. Resilication at the top of the foreland bauxite in Surinam and Guyana. Miner Deposita. 1974;9:169-73. https://doi.org/10.1007/BF00207974

Valeton I, Beissner H, Carvalho A. The Tertiary bauxite belt on tectonic uplift areas in the Serra da Mantiqueira, Southeast Brazil. Stuttgart: Contributions to Sedimentary Geology; 1991.

Valeton I, Melfi AJ. Distribution pattern of bauxites in the Cataguases area (SE Brazil), in relation to Lower Tertiary paleogeography and younger tectonics. Sci Géol Bull. 1998;41:85-98.

Yeomans JM, Bremner JC. A rapid and precise method for routine determination of organic carbon in soil. Commun. Soil Sci. Plant Anal. 1998;19:1467-1476.